JOURNAL OF SPACECRAFT AND ROCKETS
Vol. 44, No. 2, March–April 2007

Erratum

Erratum on Design of a Pulse-Facility Nozzle Using the Rotational Method of Characteristics

Richard L. Gaffney Jr.*
NASA Langley Research Center, Hampton, Virginia, 23681-2199

DOI: 10.2514/1.30729
[*J. Spacecraft*, 43(6), pp. 1216–1224 (2006)]

This paper, published in the November–December 2006 issue of *the Journal of Spacecraft and Rockets,* included a number of figures in black and white that should have published in color. The paper is reproduced here in full with the color figures. AIAA regrets the error.

A new nozzle has been designed for NASA's HYPULSE shock/expansion tube facility to be used for scramjet engine testing at a Mach-15 flight-enthalpy condition. The nozzle has an area ratio of 9.5:1 that expands the inflow from Mach 6 along the centerline to Mach 8.7 and achieves the goal of increasing the area of the core flow (by a factor of 9). The nozzle contour was generated by a new computer program that solves the Euler equations using the rotational method of characteristics. The rotational method was required to properly include the effects of the boundary layer-induced nonuniformities of the flow properties at the nozzle inflow. Although the density and Mach number vary radially at the nozzle exit due to the nonuniformities of the inflow, the new nozzle produces exit flow that is parallel and has uniform static pressure. The design has been verified with a computational fluid dynamics calculation that compares favorably with the method of characteristics solution.

Nomenclature

a	=	speed of sound
C^+	=	left running characteristic line
C^-	=	right running characteristic line
M	=	Mach number
P	=	pressure
R	=	radial coordinate of a streamline
r	=	radial coordinate
V	=	velocity magnitude
x	=	streamwise coordinate
γ	=	ratio of specific heats
δ	=	two-dimensional/axisymetric switch (0 or 1)
θ	=	flow angle
μ	=	Mach wave angle
ν	=	Prandtl–Meyer function
ρ	=	density
ϕ	=	arbitrary variable

Subscript

o	=	total condition

Presented as Paper 0691 at the 43rd AIAA Aerospace Sciences Meeting and Exhibit, Reno, Nevada, 10–13 January 2005; received 22 September 2005; revision received 6 March 2006; accepted for publication 6 March 2006.

*Aerospace Engineer, Hypersonic Air Breathing Propulsion Branch; Richard.L.Gaffney@NASA.GOV. Senior Member AIAA.

I. Introduction

WITH NASA's successful development and flight test of scramjet engine designs at Mach 7 and 10, attention has turned to the design and testing of a Mach-15 scramjet engine. Much of the Mach-10 scramjet engine testing was done in NASA's HYPULSE shock/expansion tube facility located at ATK-GASL in Ronkonkoma, New York. As the Mach-10 tests were coming to a conclusion, several runs were made at a Mach-15 flight-enthalpy condition to evaluate test possibilities for a Mach-15 scramjet engine design. The facility nozzle used in the Mach-10 tests was replaced by a conical flow nozzle that was designed for a Mach-21 flight-enthalpy aerothermodynamic test. This nozzle produced a test flow with properties that varied both radially and axially, which was undesirable for engine testing. Because the heat loads in a pulse facility are low, nozzles can be made of fiberglass and are relatively inexpensive to manufacture. With this in mind, a decision was made to design and build a new nozzle for future Mach-15 flight-enthalpy-condition tests.

While the HYPULSE facility is able to produce a wide range of flow conditions, the size of the core flow at the tube exit is usually significantly smaller than the 6 in. diameter of the tube due to the growth of the boundary layer in the tube. The solution to this problem is to expand the tube-exit flow in a nozzle. Unfortunately, the design of a nozzle for the facility operating in expansion tunnel mode is challenging because of the flow nonuniformity at the tube exit. For the new design, several options were considered for both the method and the code to be used. Korte [1] has developed a technique using Sivells's irrotational method of characteristics (MOC) code [2] for high-temperature flows in which there is significant variation in the ratio of specific heats in the nozzle. However, using Sivells's program would require significant modification to the FORTRAN 66 code to allow for Mach-6 nonuniform inflow and a rotational flowfield.

A second option was to use Korte's CAN-DO code [3] that fits the nozzle contour with a spline and adjusts the spline points to give optimal exit flow. In this code, the flowfield is analyzed with a parabolized Navier–Stokes solver. This method has the advantage that viscous effects are included in the optimization process. It has the disadvantage of being limited by the number of control points used in the optimization process, and it requires much more computer time than an MOC solver. In addition, the code must be modified for each specific case being considered.

A third option was to write a new computer program to solve the Euler equations using the rotational MOC. This option has the advantage of not being limited by the structure (or programming language) of an existing code, not having to work through a program line by line to make the necessary modifications, it is relatively fast to run, and the number of points defining the contour depends on the number of initial points (user specified). Although this option does not directly take into account viscous effects, the nonuniform profiles of the total properties entering the HYPULSE nozzle are created by viscous effects and are maintained by solving the rotational equations. Final viscous corrected contours can be generated by iterating the MOC solution with a full Navier–Stokes solution [4] (usually only one or two iterations). This paper will present the details of the rotational method of characteristics applied to general nozzle design followed by a discussion of how the computer program was applied specifically to the design of a nozzle for the HYPULSE facility.

II. Rotational Method of Characteristics

Facility nozzles for aerodynamic tests are usually designed to process flow at near stagnation conditions and produce uniform exit flow at the design Mach number. In these circumstances, all of the stagnation properties at the inflow of the nozzle are uniform. For

hypervelocity tests, stagnating the flow is not a practical solution as the total temperature is high enough to cause the flow to dissociate and the pressure is difficult to contain. Shock-expansion facilities, such as HYPULSE [5], are able to generate high-speed high-enthalpy flow without stagnating the flow. However, the HYPULSE expansion tube is only 6 in. in diameter, and viscous effects reduce the size of the usable core flow to about 3 in. or less. By processing the tube-exit flow through a nozzle, the size of the core flow can be increased allowing for larger test articles. Unfortunately, the viscous effects not only reduce the size of the core flow, they also cause the flow to be heavily profiled (nonuniform) in both static and total properties. This significantly complicates the design of the nozzle. Fortunately the method of characteristics, which has been used extensively in nozzle design, can also be used in this case.

In a supersonic isentropic nozzle flow with constant total properties, the flow is irrotational. The governing fluid equation is the compressible potential equation that can be solved using the method of characteristics. For axisymmetric flows, this involves solving two ordinary differential equations (compatibility equations) along left and right running characteristic curves (one equation along each characteristic). Equations for the two characteristic curves are solved with the two compatibility equations.

If the total conditions are nonuniform at inflow, the flow is rotational and the Euler equations must be solved. Fortunately, for supersonic isentropic flow they can also be solved using the MOC. However, there are four ordinary differential equations that must be solved along three characteristic curves. Following the work of Zucrow and Hoffman [6], the compatibility equations for the rotational MOC are

$$\rho V\,\mathrm{d}V + \mathrm{d}P = 0 \tag{1}$$

$$\mathrm{d}P - a^2\,\mathrm{d}\rho = 0 \tag{2}$$

and

$$\frac{(\sqrt{M^2-1})\,\mathrm{d}P}{\rho V^2} \pm \mathrm{d}\theta + \delta\left[\frac{\sin\theta\,\mathrm{d}x}{rM\cos(\theta \pm \mu)}\right] = 0 \tag{3}$$

The term δ in Eq. (3) is zero for two-dimensional flow and one for axisymmetric flow. Compatibility Eqs. (1) and (2) hold along the streamline whose characteristic equation is

$$\frac{\mathrm{d}r}{\mathrm{d}x} = \tan\theta \tag{4}$$

while compatibility Eq. (3) holds along left and right running Mach lines given by

$$\frac{\mathrm{d}r}{\mathrm{d}x} = \tan(\theta \pm \mu) \tag{5}$$

For calorically perfect gas flows the compatibility equations can be recast in a different form with some manipulation:

$$\mathrm{d}P_o = 0 \tag{6}$$

$$\mathrm{d}\rho_o = 0 \tag{7}$$

and

$$\mathrm{d}(\nu \pm \theta) - \frac{\mathrm{d}P_o}{\gamma P_o M^2 \tan\mu} - \delta\left[\frac{\sin\mu\sin\theta\,\mathrm{d}r}{r\sin(\theta \mp \mu)}\right] = 0 \tag{8}$$

where ν is the Prandtl–Meyer function described in [7]. This form of the equations is similar to that used by Genkin et al. [8] and has the advantage of no discretization error for the streamline compatibility equations.

Equations (6) and (7) are the compatibility equations that hold along a streamline [Eq. (4)]. These equations can be solved exactly with the result that the total conditions are constant along a streamline. Equation (8) is the compatibility equation that holds along the left and right running Mach lines [Eq. (5)]. The second term in the equation is due to the rotationallity of the flow. If the total pressure is constant in the flow, this term is zero. The third term in the equation is the axisymmetric source term. For the special case of two-dimensional irrotational flow, the second and third terms are zero and the equation can be solved exactly.

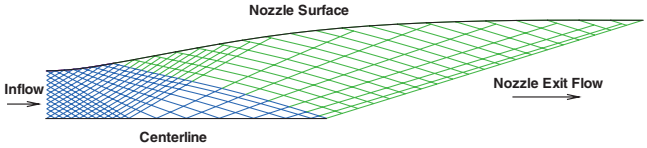

Fig. 1 Example of a characteristic net in a nozzle flowfield.

These equations are solved numerically by discretization of the equations on a grid created by intersecting characteristic lines, such as that shown in Fig. 1. The discretization of the equations is that given by Anderson [7] and involves two adjacent points in the grid. (Each equation involves its own pair of grid points.) Differentials in the equation are replaced with first-order backward differences, and all other terms are averages between the two points. For example, the second term in Eq. (8) is discretized as

$$\frac{P_{o2} - P_{o1}}{\gamma \bar{P}_o \bar{M}^2 \tan\bar{\mu}} \tag{9}$$

where the overbar denotes the arithmetic average

$$\bar{\phi} = \frac{\phi_1 + \phi_2}{2} \tag{10}$$

Each equation is discretized along the appropriate characteristic curve and involves one known point and one unknown point, which results in a system of coupled nonlinear algebraic equations that are solved simultaneously using a Newton–Raphson method. Because the governing equations for steady supersonic inviscid flow are hyperbolic, solution points can be computed sequentially. For nozzle design, the solution at points that depend on the inflow and the user-specified expansion portion of the nozzle (the blue region in Fig. 1, also called the kernel) are computed first. The turning contour and the points dependent on it (the green region in Fig. 1) are then computed. The solution procedure at each point depends on the type of point being solved, interior, centerline, surface point, etc. The unit processes for interior, centerline, and known surface points are detailed in the textbook by Zucrow and Hoffman [6]. The unit processes for determining the turning contour were developed by the author. For completeness, each of the unit processes is discussed below.

A. Interior Point

The solution geometry of an interior point in the kernel is illustrated in Fig. 2. The location and properties of points 1 and 2 are known. Point 4, which is the new point, is located at the intersection of the C^+ characteristic running through point 1 and the C^- characteristic running through point 2. Point 3 lies at the intersection of the line connecting points 1 and 2 and the streamline passing through point 4. The properties at point 3 are linearly interpolated from points 1 and 2. Given this geometry, Eqs. (1–3) are discretized using the appropriate points. The resulting equation set is then solved, yielding the location and properties of point 4 (and point 3 in the process).

B. Centerline Point

The solution geometry of a point on the centerline is illustrated in Fig. 3. The location and properties of points 1 and 2 are known. Point 3, which is the new point, is located at the intersection of the C^- characteristic running through point 2 and the centerline ($r = 0$), which is also a streamline. The compatibility equation along the C^+ characteristic is replaced by the boundary condition $\theta_3 = 0$. Because the centerline is also a streamline, the total properties at point 3 equal the total properties at point 1 leaving only one unknown property (M)

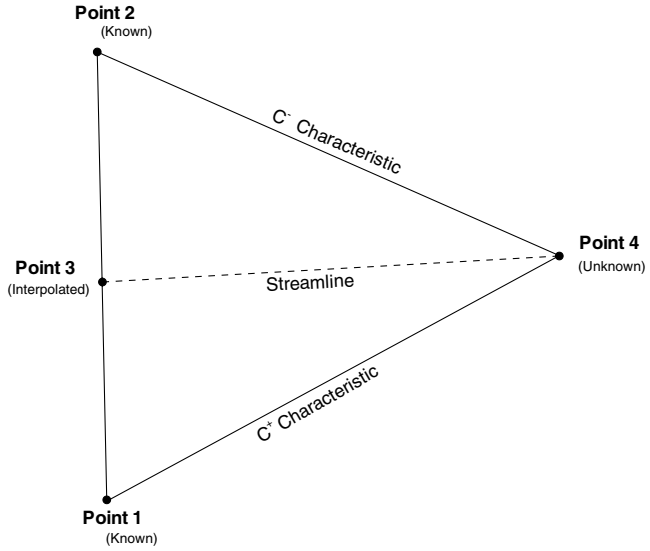

Fig. 2 Schematic of the interior kernel-point geometry.

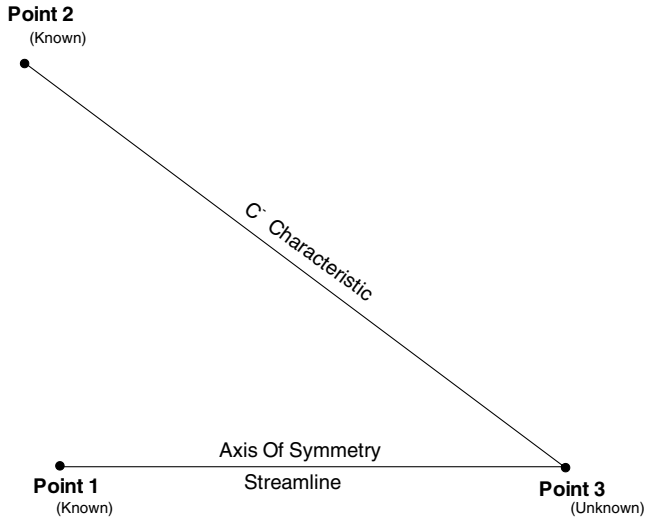

Fig. 3 Schematic of a centerline point geometry.

that is determined by solving the compatibility equation along the C^- characteristic.

C. Nozzle Surface

The solution geometry of a point on the nozzle surface in the user-specified expansion region is illustrated in Fig. 4. The location and properties of points 1 and 2 are known. Point 3, which is the new point, is located at the intersection of the C^+ characteristic running through point 1 and the known nozzle surface, which is also a streamline. For this type of solution geometry the C^- compatibility equation is replaced by the boundary condition

$$\theta_3 = \left.\frac{\mathrm{d}r}{\mathrm{d}x}\right|_{\text{nozzle surface}} \tag{11}$$

Because point 3 lies on the same streamline as point 2, the total properties at point 3 equal the total properties at point 2. The remaining properties at point 3 are determined by simultaneously solving the compatibility equation along the C^+ characteristic and determining the intersection of the C^+ characteristic with the given nozzle surface, $r = f(x)$.

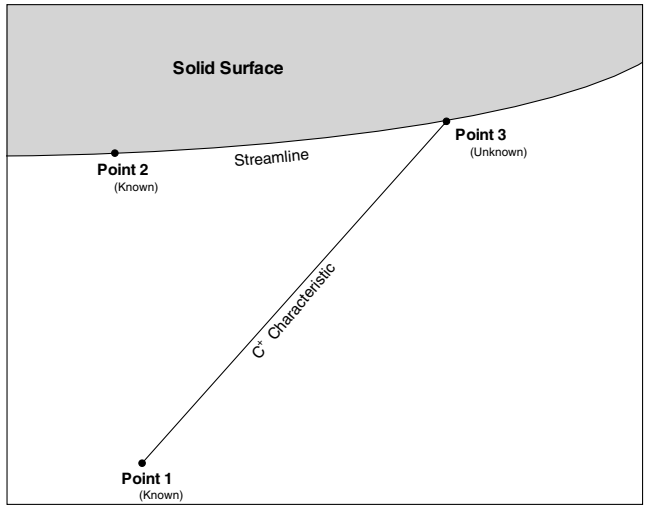

Fig. 4 Schematic of a solid surface point geometry.

D. Final C^+ Characteristic

Once points in the kernel have been computed, points in the turning region can be computed. This is accomplished by first computing the solution at a point on the final (terminating) C^+ characteristic. The point arrangement of this solution step is illustrated in Fig. 5. The solutions at points 1, 2, and 3 are known. Point 5 is the new unknown point. It is located at a user-specified distance from point 1 along the final characteristic. Point 4 is located at the intersection of the line between points 2 and 3 and the streamline running through point 5. The properties at point 4 are linearly interpolated from points 2 and 3. Because there is no C^- characteristic, the user is free to specify one flow property. The solution of the resulting equation set yields the properties at point 5 (and point 4).

Ideally, one would like the nozzle exit flow to be parallel and be as uniform as possible. If the user specifies that $\theta = 0$ along the final characteristic, Eq. (3) gives $\mathrm{d}P = 0$, and the flow at the nozzle exit is both parallel and has uniform static pressure.

E. Interior Point, Turning Contour

Once the solution of a point on the final characteristic has been computed, points in the interior are computed sequentially, moving from the final characteristic upstream along a C^- characteristic to the nozzle surface. The geometry for this situation is shown in Fig. 6. The solutions at points 1, 2, 3, and 4 are known whereas the solution at point 6 is unknown. Point 6 is located at the intersection of the C^- characteristic running through point 1 and the C^+ characteristic running through point 2. Point 5 is located at the intersection of the line connecting points 3 and 4 and the streamline running through point 6. The properties at point 5 are linearly interpolated from points 3 and 4. The solution of the discretized equations yields the properties at point 6 (and point 5).

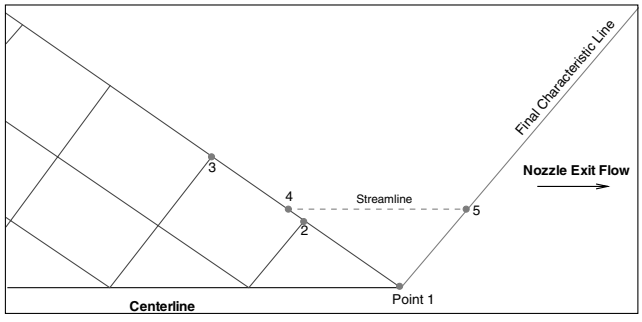

Fig. 5 Schematic of a final characteristic point geometry.

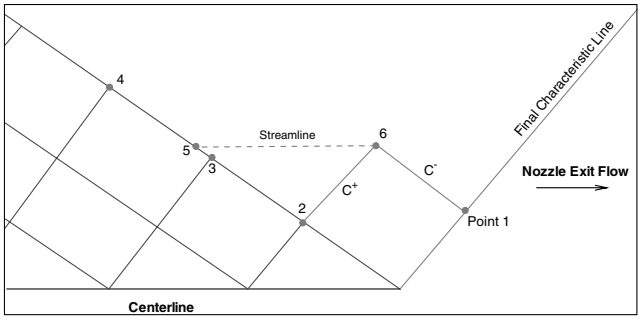

Fig. 6 Schematic of an interior point (turning region) geometry.

F. Surface Point, Turning Contour

As stated previously, the solution of interior points in the turning region starts at the final characteristic and progresses upstream along the C^- characteristic. Near the nozzle surface, a place is reached where the new point, located at the intersection of the C^+ and C^- characteristics, lies outside of the flowfield. This situation is recognized when the computer program cannot find any points on a streamline upstream of the new point. When this happens, the new point must be a surface point, which is shown graphically in Fig. 7. In this case, points 1 and 2 are known and point 3 is the new unknown surface point. The surface point is positioned along the C^- characteristic that runs through point 1 at a location where the mass flow computed (using the trapezoidal rule) along the C^- characteristic matches the mass flow at inflow. The line connecting points 2 and 3 is the surface, which is also a streamline. The solution of the discretized equations and the mass flow requirement yields the properties and location of point 3.

After a surface point is computed, the solution procedure returns to the final characteristic and computes a new row of points along the next C^- characteristic. This procedure is repeated until the surface and the final characteristic intersect.

G. Numerical Considerations

There are several sources of error that are introduced as part of the numerical process. This includes both discretization errors and convergence errors. The discretization errors are fixed by the desire to limit the number of points associated with each calculation, which greatly reduces the complexity of solving Eqs. (4–8). Convergence errors are limited by applying the iterative procedure at each unknown point until the absolute value of the maximum residual of Eqs. (6–8) is less than 1.0×10^{-10}.

Because the numerical scheme is sequential in nature, errors can build up as the solution progresses downstream. At the higher Mach numbers, where the characteristic lines are long and very shallow, these errors can produce small perturbations in the contour near the end of the nozzle (where the Mach number is highest). In high-Mach-number flows these irregularities, which may be too small to detect with the human eye, can produce pressure waves and nonuniform flow at the nozzle exit. To avoid this, the first and second derivatives of the nozzle contour are examined as a post processing step. If perturbations are identified, the contour near the exit is smoothed using a Savitzky–Golay smoothing filter [9].

One other problem that can occur in an MOC solution is that of characteristic lines of the same family converging. This situation occurs when a shock wave forms in the flowfield (which violates the MOC isentropic flow assumption). The convergence can also be the result of numerical errors. If characteristic lines are close together, small errors can cause them to converge or even cross. This problem tends to occur when the user, in an attempt to reduce discretization errors, uses a large number of characteristics in the calculation. Whether real or numerical, dealing with converging or crossing characteristic lines increases the complexity of the solution procedure. The current program handles crossed C^+ characteristic lines near the nozzle exit by dropping one of the lines from the characteristic net. If more than two lines converge or cross, the program stops.

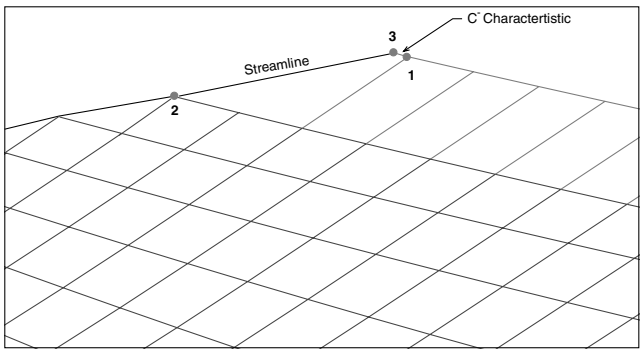

Fig. 7 Schematic of a surface point (turning region) geometry.

H. MOC Verification

The first step in the verification process was to verify that the new rotational MOC code could reproduce a nozzle contour generated by an irrotational MOC code (using uniform inflow properties). This was done using an irrotational MOC code, also written by the author. The contours generated by the two codes were nearly identical, differing only by a very small amount caused by the difference in the truncation error of the two solution methods. (The irrotational assumption leads to a simplification of the governing equations and the solution method.) The two contours were also verified using inviscid CFD. These comparisons are omitted here for brevity.

The second step in the verification of the MOC code was done by designing a nozzle with a nonuniform inflow. The inflow conditions were a constant static pressure and static density of 200 kPa and 0.5 kg/m^3, respectively, and a Mach number that varied linearly from 2.0 at the centerline to 1.01 at the wall. These conditions result in nonlinear profiles of total pressure and total density as shown in Fig. 8. The target nozzle was designed to have a centerline exit Mach number of 5.0, a constant exit static pressure, and parallel exit flow. For this case the gas constant was set to 287.06 $J/(kg \cdot K)$, and γ was set to 1.4. The initial expansion surface (from the throat to the inflection point) was specified as a Gaussian curve with a radius of curvature at the throat of 5.0. For these conditions, the exit profiles can be determined analytically. By design, the exit flow angle is zero and the static pressure is constant. From the isentropic nature of the flowfield, the exit total pressure and total density profiles are similar to those at the nozzle inflow, having the same values (along a streamline) but different radial distributions. The relationship

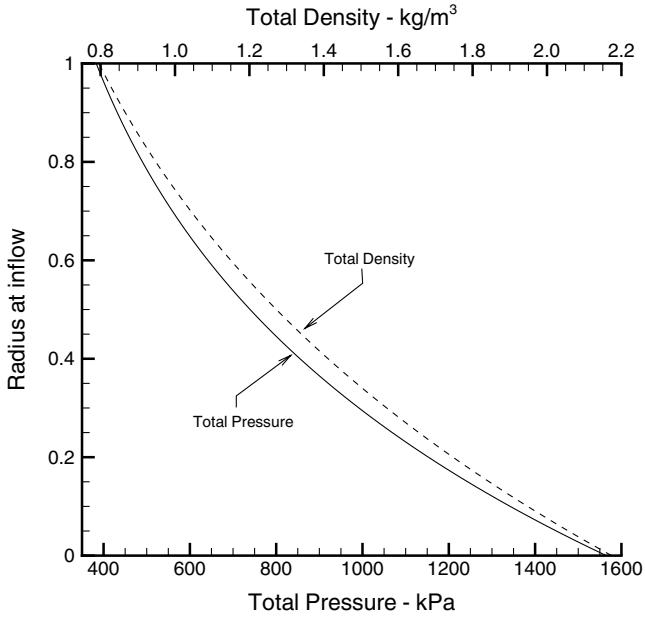

Fig. 8 Verification-case total pressure and total density inflow profiles.

between the radius of an inflow streamline (R_{inflow}) and the radius of the same streamline at the nozzle exit (R_{exit}) can be derived from the conservation of mass and is

$$R_{\text{exit}}^2 = 2\sqrt{\frac{P_{\text{inflow}}}{P_{\text{exit}}}}\int_0^{R_{\text{inflow}}}\left[\sqrt{\frac{\rho_{\text{inflow}}}{\rho_{\text{exit}}}}\left(\frac{M_{\text{inflow}}}{M_{\text{exit}}}\right)r\right]\mathrm{d}r \qquad (12)$$

where M_{inflow} is a known distribution. By equating the exit total pressure to the inflow total pressure (along a streamline) the following relationship between the inflow and exit Mach numbers can be derived:

$$M_{\text{exit}} = \sqrt{\frac{2}{\gamma-1}\left\{\left(\frac{P_{\text{inflow}}}{P_{\text{exit}}}\right)^{\frac{\gamma-1}{\gamma}}\left[1+\left(\frac{\gamma-1}{2}\right)M_{\text{inflow}}^2\right]-1\right\}} \qquad (13)$$

For a constant inflow density, the density ratio is

$$\frac{\rho_{\text{inflow}}}{\rho_{\text{exit}}} = \left(\frac{P_{\text{inflow}}}{P_{\text{exit}}}\right)^{\frac{1}{\gamma}} \qquad (14)$$

which is constant, allowing the density ratio to be moved outside of the integral in Eq. (12). For the more general case where the inflow density varies, the density ratio can be determined by setting the total density at inflow to that at the exit (along a streamline) giving

$$\frac{\rho_{\text{inflow}}}{\rho_{\text{exit}}} = \left\{\frac{1+[(\gamma-1)/2]M_{\text{exit}}^2}{1+[(\gamma-1)/2]M_{\text{inflow}}^2}\right\}^{\frac{1}{\gamma-1}} \qquad (15)$$

For an inflow radius of 1.0 and a centerline exit Mach number of 5.0, the theory gives an exit radius of 3.4199 and an exit static pressure of 2957.7 Pa. (Recall that the length scale is not a governing parameter in an inviscid flow and so the units of length are arbitrary. For inviscid calculations in the current work, all lengths are measured in inflow radii. For viscous calculations the contour is scaled to the actual physical size.)

Six nozzle contours were generated using the MOC with 15, 31, 65, 97, 135, and 201 inflow points. Smoothing of the contour was not needed for these cases. The error in the exit radius decreased monotonically from 0.0328 for the 15 point case to 0.00285 for the 201 point case, which corresponds to less than 1% error for the 15 point case and less than 0.1% error for the 201 point case. In all cases the exit static pressure exactly matched the theoretical value. A sample of the contour generated by the MOC is shown in Fig. 9. (On this scale all six contours look identical.) Figure 10 shows the total pressure profiles at the nozzle exit for the theory and for the MOC cases with 15, 31, and 65 points. (The other MOC profiles were very close to the theoretical curve and were left off the figure for clarity.) The maximum error in the total pressure profiles ranges from about 7.7% for the 15 point case to less than 0.6% for the 201 point case. The Mach number profiles at the nozzle exit were computed from the static and total pressures and are shown in Fig. 11. The maximum error in Mach number varied from about 1.35% for the 15 point case to about 0.11% for the 201 point case.

The order of accuracy of the method was determined by plotting the $\log_{10}$ of the error in the exit radius versus the $\log_{10}$ of the number of inflow points (see Fig. 12). The slope of the line verifies that this method is first-order accurate.

Although the theory is useful for evaluating the MOC exit radius and exit properties, it does not provide any information on the quality of the MOC generated contour. Instead, CFD calculations on three grids were used. The three grid dimensions were 201×65, 401×129, and 801×257, where the first number is the number of points in the streamwise direction and the second number is the number of radial points. The contour used to generate the grids was computed by the MOC code using 65 inflow points. All three solutions were computed with the VULCAN code [10], and the L_2 norm of the error reduced 14 orders of magnitude. The calculations were done assuming inviscid calorically perfect flow. Contours of the $\log_{10}$ of the static pressure are depicted in Fig. 13, which shows

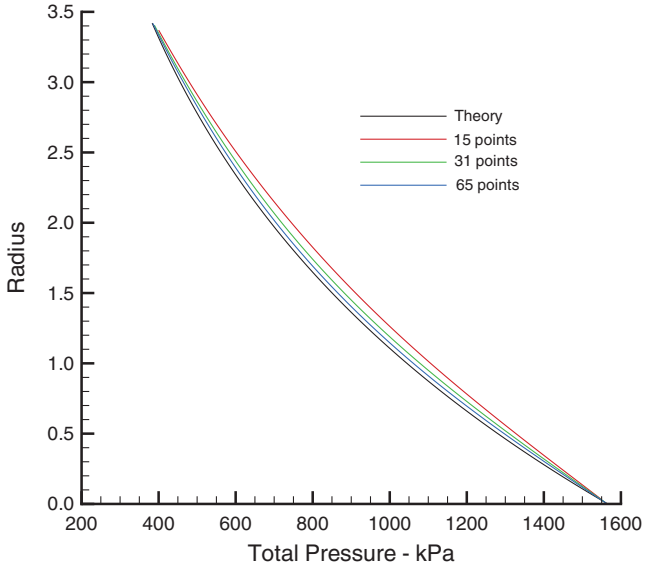

Fig. 10 Theoretical and MOC total pressure profiles at the nozzle exit.

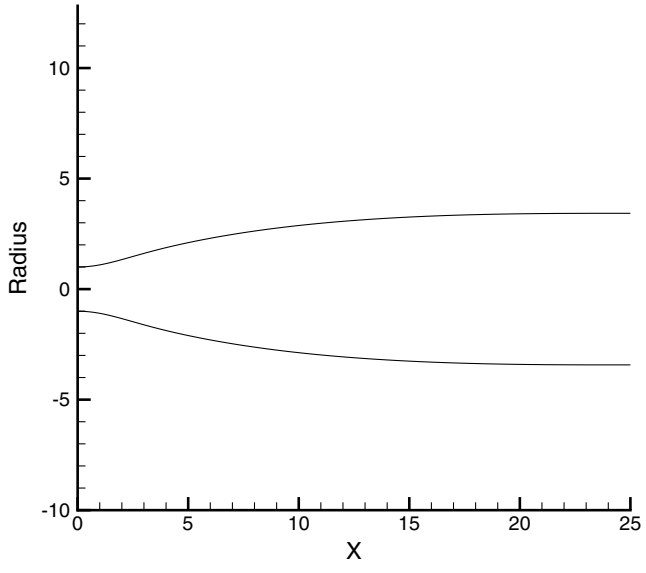

Fig. 9 Verification-case MOC contour.

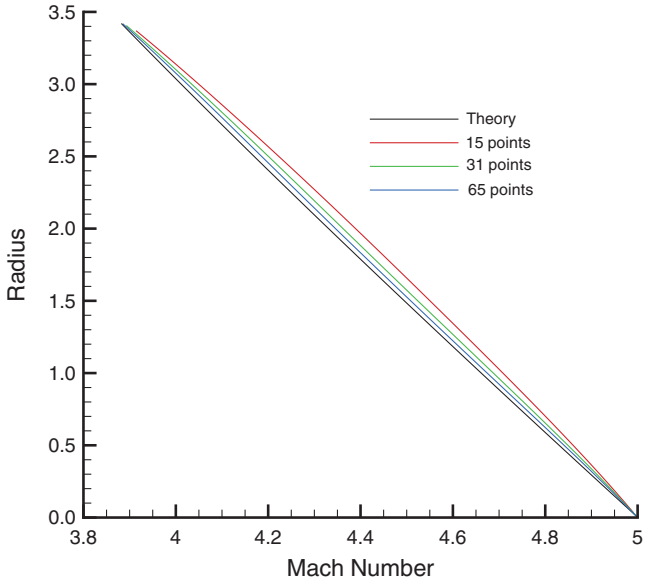

Fig. 11 Theoretical and MOC Mach number profiles at the nozzle exit.

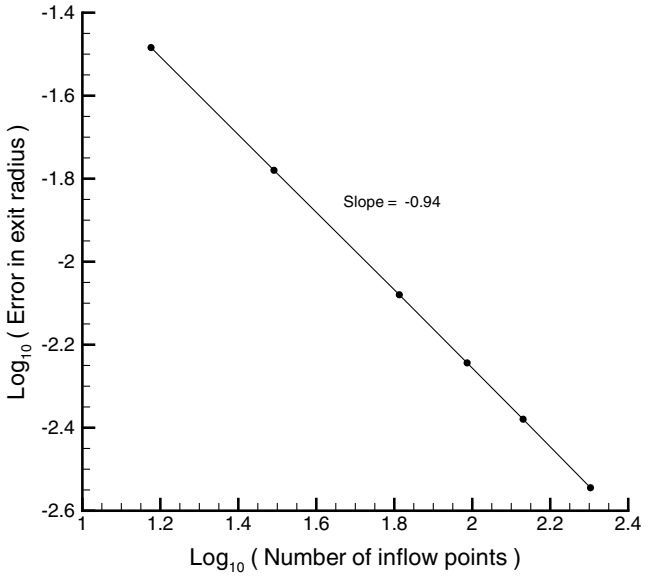

Fig. 12 Error in exit radius vs number of points, convergence property.

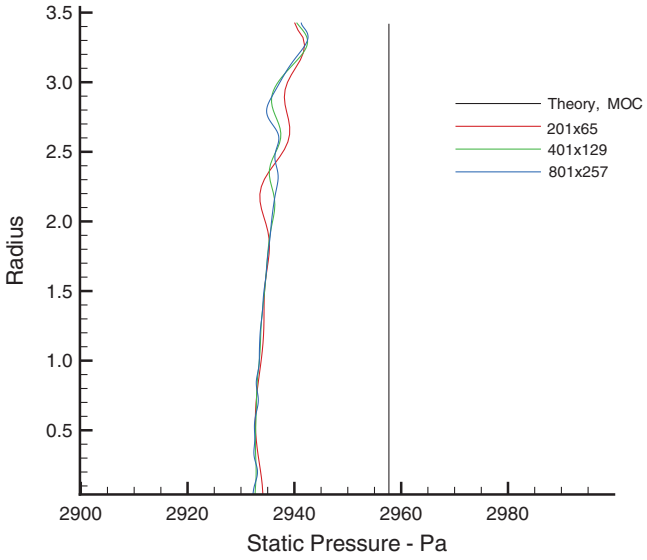

Fig. 14 Theoretical, MOC, and CFD static pressure profiles at the nozzle exit.

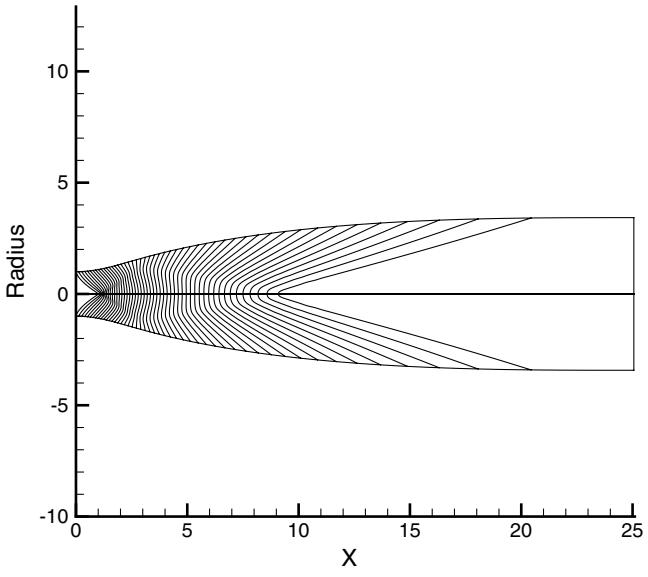

Fig. 13 CFD contours of $\log_{10}$ (static pressure) in the nozzle.

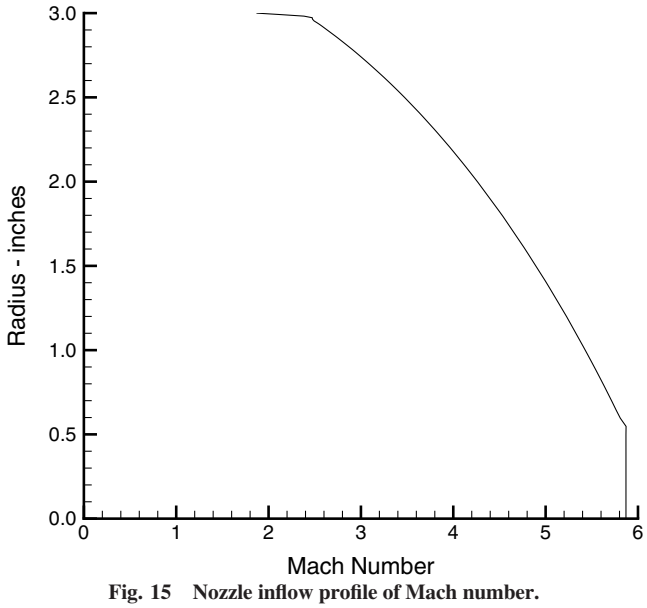

Fig. 15 Nozzle inflow profile of Mach number.

that the flow is accelerated smoothly to a constant static pressure without wave reflections. The maximum error in the exit total pressure profile for all three CFD solutions is less than 0.3% whereas the static pressure, shown in Fig. 14, is low by about 20 Pa (0.67%). Although low, the CFD computed static pressure is very uniform having a variation of only 0.34%. For all three CFD cases, the Mach number is high by about 0.15%. The slightly high Mach numbers and low static pressures are consistent with an exit radius that is slightly higher than the theoretical value. These low values of error verify the MOC nozzle design procedure and code.

III. HYPULSE Nozzle Design

The HYPULSE facility is a shock/expansion tube pulse facility [5]. A shock wave is generated by rupturing a diaphragm separating tube sections with different fill pressures. As the shock wave travels the length of the tube, it imparts energy (velocity, pressure, and temperature) to the gas. In expansion tube mode, a second diaphragm (with a third tube section) is used to increase the strength of the shock wave and create an unsteady expansion fan that generates very high-enthalpy flow. The advantage of this type of facility is that it is able to generate very high-enthalpy flow without stagnating the test gas. One disadvantage is the short test times (tens of milliseconds or less). In this type of facility, the test time is generally proportional to the tube lengths. Although long tubes are desirable for longer test times, viscosity creates a boundary layer that reduces the test time and the size of the test core. Fortunately the core size can be increased by expanding the tube-exit flow through a nozzle.

The procedure for the design of the nozzle for the HYPULSE facility is similar to that for the verification-case nozzle. In this case, the inflow conditions were derived from an experimental pitot pressure profile of the HYPULSE tube exit at a Mach-15 flight-enthalpy condition (see the acknowledgments). The Mach number and static density were computed from the pitot profile assuming a constant static pressure of 198,215 Pa and a Crocco–Busemann temperature-velocity relationship [11]. The inflow profiles of Mach number and static density are shown in Figs. 15 and 16, respectively. The inflow was assumed to be parallel. At these operating conditions, there is only a 1.2 in. diameter core at the tube exit. As in the verification case, the expansion surface of the nozzle was specified as a Gaussian curve, with the radius of curvature at the inflow and the slope of the surface at the inflection point set by the user. For parallel exit flow, the specification of the expansion surface is the only input the user has in the design.

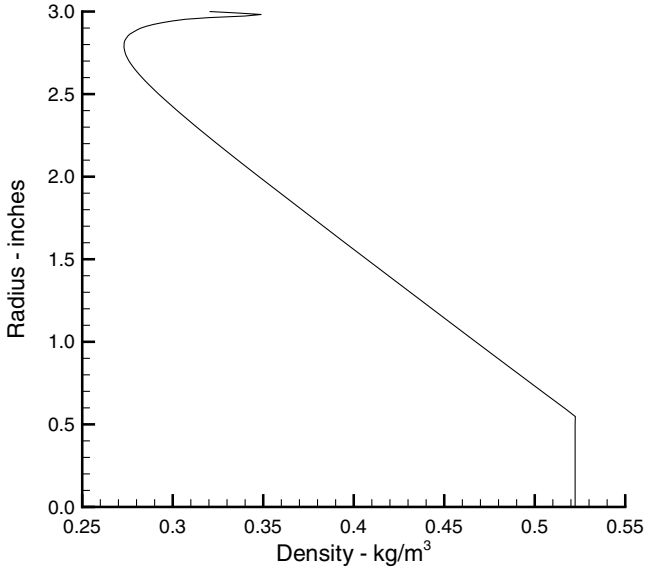

Fig. 16 Nozzle inflow profile of density.

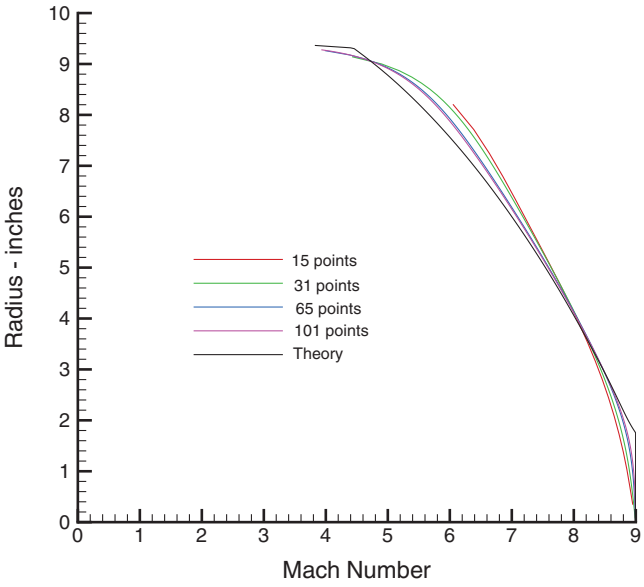

Fig. 18 Theoretical and MOC Mach number profiles at the nozzle exit.

Although the user input is limited to specifying the radius of curvature and the inflection point slope, several tradeoffs must be considered in the nozzle design process. On one hand, increasing the slope at the inflection point leads to a higher centerline exit Mach number and a longer nozzle. On the other hand, a small radius of curvature results in faster expansion of the flow and a shorter nozzle. However, viscous effects must also be considered. A long nozzle has a thicker boundary layer and a smaller core-flow size, whereas the rapid expansion of a nozzle with a small radius of curvature (shorter nozzle) can perturb or even separate the boundary layer introducing nonuniformities into the core flow. In addition, an MOC design with parallel exit flow always has a zero slope at the nozzle exit. In a viscous flow, the streamlines are displaced by the boundary layer, and the flow near the MOC nozzle exit begins to recompress. As a result MOC designs are usually corrected for the boundary layer or truncated, which must be taken into account during the design process.

One other consideration in the design process is the nonuniformity of the nozzle inflow. Because total properties are constant along a streamline [Eqs. (6) and (7)], any nonuniformities in these properties present at inflow will also be present at outflow.

The goal of the nozzle design effort was to produce a nozzle contour that, for the given tube-exit profiles, produced acceptable conditions for testing a generic Mach-15 scramjet engine flowpath. Inlet entrance conditions were derived from an analysis of the forebody flowfield of a generic airbreathing launch vehicle flying at Mach 15. There was some flexibility in setting the target nozzle exit conditions based on the inlet conditions because the angle of attack of the test article could be varied to further process the flow between the nozzle exit and the engine inlet. To map the possible solution space, three nozzles with parallel exit flow and constant exit static pressures were designed with centerline exit Mach numbers of approximately 9, 9.5, and 10. Upon review of the solutions, the Mach-9 nozzle was selected.

The characteristic net and nozzle contour are shown in Fig. 17. This design was generated with a radius of curvature at inflow of 6 in. and a slope of 4.4 deg at the inflection point. A γ of 1.32 was used that was representative of values computed in a quasi-one-dimensional calculation with a variable thermodynamics model. (The variation of γ in a nozzle affects the exit Mach number and, to a lesser degree, flow uniformity. For constant γ designs, the exit Mach number can be achieved by adjusting the exit area, whereas flow nonuniformity can be minimized by selecting an appropriate value of γ. In the present work a value of 1.32 was found to be adequate.) The Mach-9 MOC contour is 98.4 in. long and has an area ratio of 9.6:1. Several contours were generated for this centerline exit Mach number using 15, 31, 65, and 101 inflow points. The exit Mach number profiles for each case are shown in Fig. 18 along with that from the theory [Eqs. (12), (13), and (15)]. It is clear from this figure that the series of MOC designs has not converged to give the theoretical exit properties. Attempts to run cases with significantly larger numbers of inflow points were unsuccessful due to crossed characteristics. The differences between the MOC profiles and the theoretical profiles are generally in the regions of slope discontinuities in the theoretical profile. These discontinuities are the result of line segments drawn through the scatter of experimental data of the inflow profile. A better convergence may have been achieved had the inflow profile been smooth.

To determine the quality of the contour generated using 101 inflow points, the nozzle flowfield was computed using CFD. Because the MOC contour had small protrusions of about 0.003 in. (and smaller), the contour was smoothed before generating the CFD grid. Figure 19 shows the slope of the surface before and after smoothing. Three inviscid constant γ (1.32) CFD calculations were done with grid dimensions of 201×65, 401×129, and 801×257. A weak

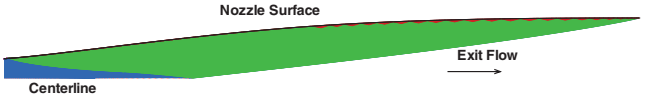

Fig. 17 Final MOC design.

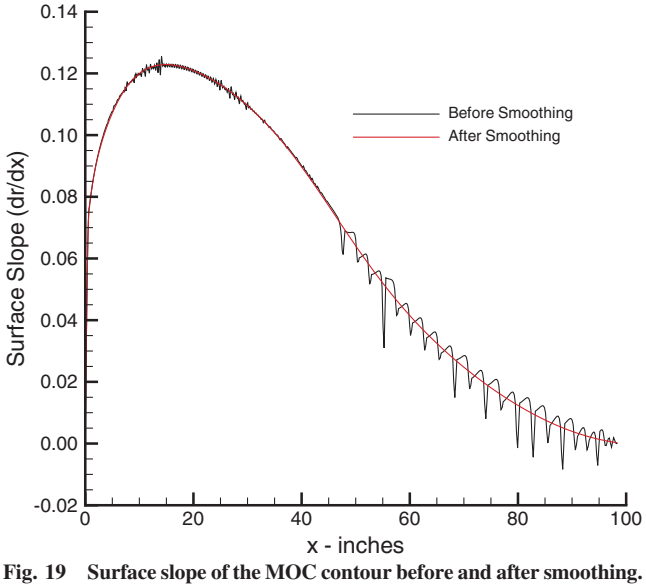

Fig. 19 Surface slope of the MOC contour before and after smoothing.

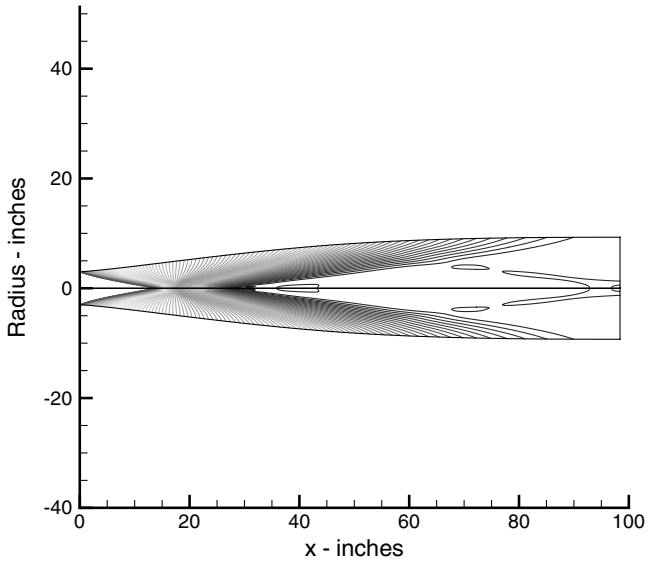

Fig. 20 CFD contours of the $\log_{10}$ (static pressure) in the final design nozzle.

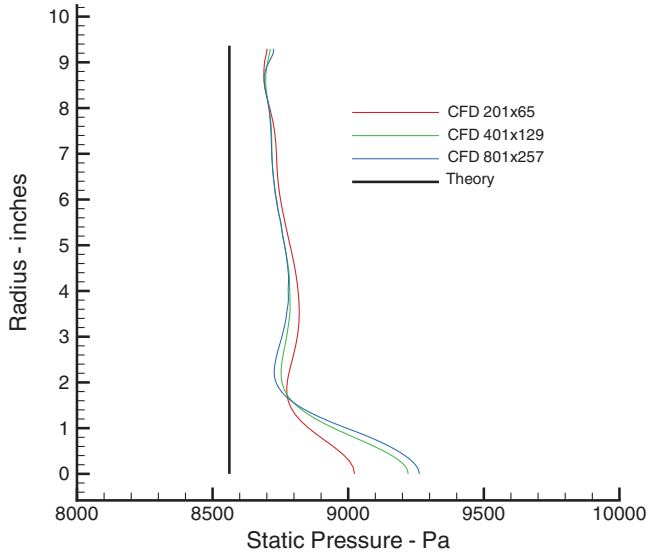

Fig. 21 CFD, MOC, and theoretical pressure profiles at the nozzle exit.

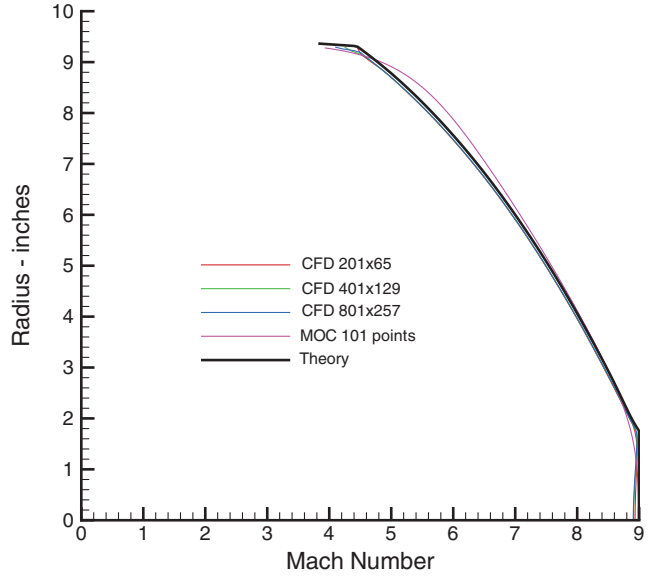

Fig. 22 CFD, MOC, and theoretical Mach number profiles at the nozzle exit.

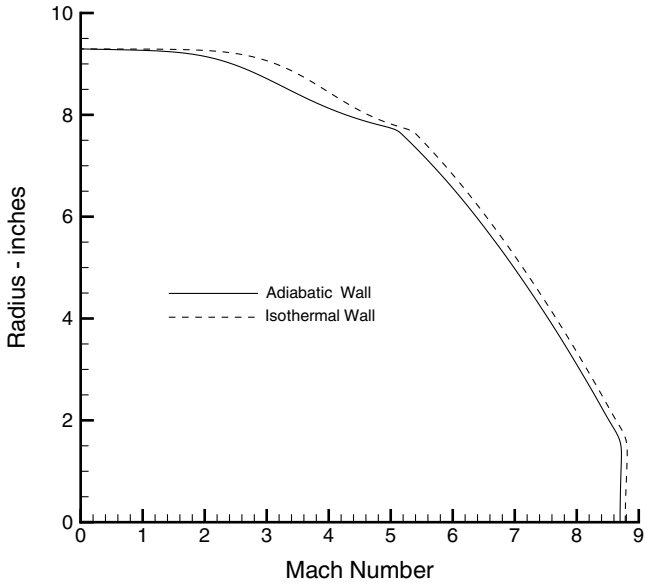

Fig. 23 CFD Mach number profies at the nozzle exit.

uncanceled pressure wave can be seen in Fig. 20, which shows contours of the $\log_{10}$ of the static pressure. The exit static pressure profiles for all three CFD cases and the theory are shown in Fig. 21. The static pressures of the CFD solutions are about 2% higher than the theoretical value for most of the exit profile but are about 6% higher near the centerline. The exit Mach number profiles are shown in Fig. 22 for the CFD solutions, the MOC solution (with 101 points), and the theory. It is interesting to note that the exit Mach number profiles from the CFD solutions match the theoretical profile better than the MOC profile.

The flowfield in the nozzle was also computed using viscous variable-γ CFD for both an adiabatic wall boundary condition and an isothermal boundary condition with the wall temperature set to 300 K. Both solutions were converged at least 10 orders of magnitude using a 301×201 grid. The Mach number profiles at the exit for the two cases are shown in Fig. 23. The difference in the profiles is due to the thicker boundary layer of the adiabatic wall case. The centerline exit Mach number for the adiabatic wall case is 8.7, whereas it is 8.78 for the isothermal wall case. Both cases have a core flow (defined by a 1% variation in Mach number) of about 3.6 in. in diameter, which is less than the theoretical value of 3.844. The static pressure profiles, shown in Fig. 24, have a pressure variation of about

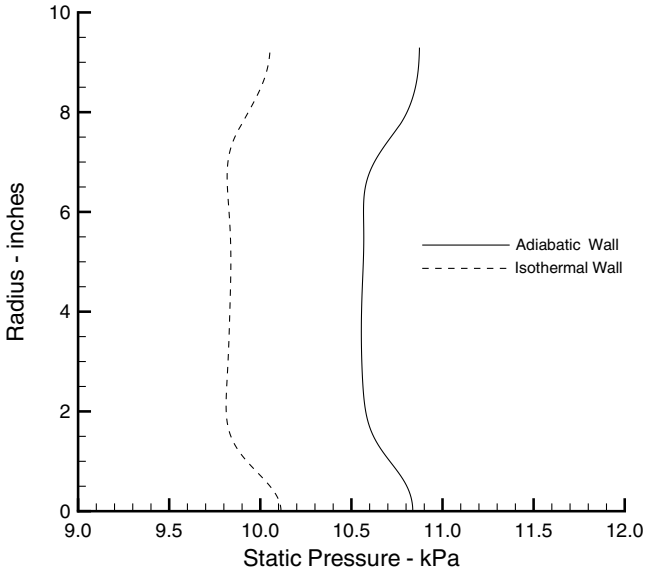

Fig. 24 CFD pressure profiles at the nozzle exit.

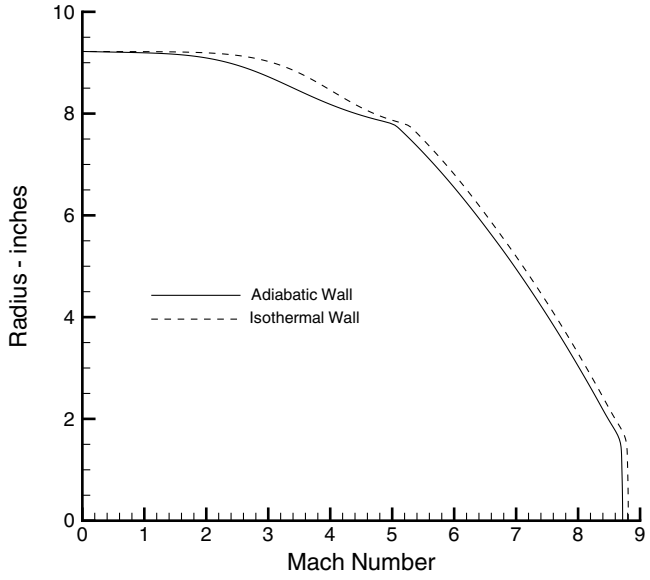

Fig. 25 CFD Mach number profiles at 82 in.

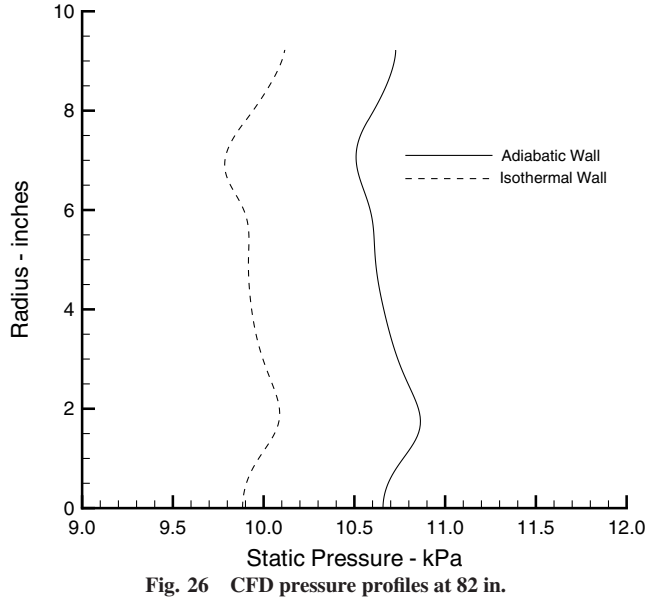

Fig. 26 CFD pressure profiles at 82 in.

3%, which is less than the exit pressure variation in the inviscid solution. This result may be due to the boundary-layer displacement thickness smoothing the contour or viscous damping of weak uncanceled pressure waves.

As mentioned previously, MOC contours have a slope of zero degrees at the nozzle exit (for parallel exit flow). For viscous flow, the boundary layer displaces the streamlines, and the flow near the exit begins to recompress. As a result the inviscid MOC contour is usually corrected by adding the displacement thickness at each axial location to the contour radial coordinate. An alternative is to simply truncate the nozzle at a point before the flow begins to recompresses and where the flow is still relatively uniform. For the current work the nozzle was truncated 82 in. from the inflow without any attempt to correct the centerline exit Mach number (the properties at this location were within the acceptable range). At the 82 in. location, the radius is 9.22 in., and the area ratio is 9.45. Profiles for the Mach number and static pressure at this location are shown in Figs. 25 and 26. At this axial location the centerline Mach numbers are slightly higher than at the exit: 8.72 for the adiabatic flow and 8.81 for the isothermal flow. Similarly, the pressures dropped about 0.3%, whereas the variation in the pressure profiles stayed about the same (3%).

IV. Conclusion

A new computer program has been written to design high-speed nozzles with nonuniform inflow profiles using the rotational method of characteristics. The program has been verified for a test case with a linear Mach number variation. The program has been successfully applied to the design of a new nozzle for the HYPULSE shock-tube facility operating at a Mach-15 flight-enthalpy test condition. Although the method of characteristics exit solution did not fully converge to the theoretical inviscid exit properties, the exit profiles were acceptable. The effects of the boundary layer were to reduce the centerline exit Mach number, increase the exit static pressure, and create a variation in the exit pressure profile of about 3%. The goal of increasing the test core size was achieved, increasing the core flow diameter from about 1.2 in. at inflow to about 3.6 in. at the exit (a factor of 9 increase in area).

Acknowledgment

R. Clayton Rogers of the NASA Langley Research Center, Hypersonic Airbreathing Propulsion Branch provided the inflow profiles for the HYPULSE nozzle design.

References

[1] Korte, J. J., "Inviscid Design of Hypersonic Wind Tunnel Nozzles for a Real Gas," AIAA Paper 2000-0677, Jan. 2000.

[2] Sivells, J. C., "Aerodynamic Design of Axisymmetric Hypersonic Wind-Tunnel Nozzles," *Journal of Spacecraft and Rockets*, Vol. 7, No. 11, Nov. 1970, pp. 1292–1299.

[3] Korte, J. J., Kumar, A., Singh, D. J., and White, J. A., "CAN-DO—CFD-Based Aerodynamic Nozzle Design and Optimization Program for Supersonic Hypersonic Wind Tunnels," AIAA Paper 92-4009, July 1992.

[4] Gaffney, R. L., Jr., and Korte, J. J., "Analysis and Design of Rectangular-Cross-Section Nozzles for Scramjet Engine Testing," AIAA Paper 2004-1137, Jan. 2004.

[5] Guy, R. W., Rogers, R. C., Puster, R. L., Rock, K. E., and Diskin, G. L., "The NASA Langley Scramjet Test Complex," AIAA Paper 96-3243, July 1996.

[6] Zucrow, M. J., Hoffman, J. D., *Gas Dynamics*, Vol. II, Wiley, New York, 1977.

[7] Anderson, J. D., Jr., *Modern Compressible Flow With Historical Perspective*, McGraw–Hill, New York, 1982.

[8] Genkin, L., Baer, M., and Falcovitz, J., "Gasdynamic Approach to Small Plumes Computation," *Journal of Spacecraft and Rockets*, Vol. 31, No. 4, July–Aug. 1994, pp. 691–700.

[9] Press, W. H., Teukolsky, S. A., Vetterling, W. T., and Flannery, B. P., *Numerical Recipes in FORTRAN, The Art of Scientific Computing*, 2nd ed., Cambridge Univ. Press, New York, 1992.

[10] White, J. A., and Morrison, J. H., "A Pseudo-Temporal Multi-Grid Relaxation Scheme for Solving the Parabolized Navier-Stokes Equations," AIAA Paper 99-3360, June 1999.

[11] Chue, R., "CFD Calculation of HYPULSE SET Nozzle for Mach 15-H16 Condition," GASL Research and Advanced Development TN 158, July 2003.

R. Cummings
Associate Editor